Desalination and Water Treatment
www.deswater.com
doi: 10.1080/19443994.2014.963149

56 (2015) 2485–2501
November

Taylor & Francis
Taylor & Francis Group

Equilibrium, kinetic and thermodynamic studies for the removal of Zn(II) and Ni(II) ions using magnetically recoverable graphene/Fe_3O_4 composite

A. Muthukrishnaraj[a], J. Manokaran[a], M. Vanitha[a], K.V. Thiruvengadaravi[b], P. Baskaralingam[b], N. Balasubramanian[a,*]

[a]*Department of Chemical Engineering, A.C Tech Campus, Anna University, Chennai 600025, India, Tel. +91 9787063528; email: muthukrishnaraj@gmail.com (A. Muthukrishnaraj), Tel. +91 9629215606; email: manokaranj86@gmail.com (J. Manokaran), Tel. +91 9677624598; email: vanithachel@gmail.com (M. Vanitha), Tel. +91 9444954151; email: nbsbala@annauniv.edu (N. Balasubramanian)*
[b]*Department of Applied Science and Technology, A.C Tech Campus, Anna University, Chennai 600025, India, Tel. +91 9003169766; email: thiruvengat.ravi@gmail.com (K.V. Thiruvengadaravi), Tel. +91 9884420351; email: baskaralingam@gmail.com (P. Baskaralingam)*

Received 31 December 2013; Accepted 26 August 2014

ABSTRACT

Magnetically recoverable graphene/Fe_3O_4 composite (GFC) was synthesized using a one-step solvothermal method by the simultaneous reduction of graphene oxide (GO) to graphene and $FeCl_3{\cdot}6H_2O$ to Fe_3O_4, in the presence of ethylene glycol and sodium acetate. The synthesized GFC adsorbent was characterized using FTIR, Raman, X-ray powder diffraction analysis, scanning electron microscopy, energy dispersive analysis of X-ray, thermo gravimetric analysis and vibrating sample magnetometer. The adsorption of Zn(II) and Ni(II) ions onto GFC has been investigated using batch adsorption studies. The adsorption experiments were carried out to examine the influence of parameters such as pH, GFC dosage, initial metal ion concentration, temperature and contact time. The adsorption isotherm data were fitted in the order of Langmuir > Redlich–Peterson > Temkin > Freundlich, based on the correlation coefficient values. From the Langmuir isotherm model, the maximum adsorption capacity of the GFC adsorbent towards Zn(II) and Ni(II) ions was found to be 121.5 and 111.4 mg g^{-1}, respectively. The adsorption kinetics follows the pseudo-second-order model, and the ΔG° and ΔH° values suggest that the adsorption of Zn(II) and Ni(II) ions onto GFC was spontaneous and endothermic.

Keywords: GFC; Zn(II) adsorption; Ni(II) adsorption; Easily recoverable; Competitive adsorption

1. Introduction

Hazardous heavy metals from industrial waste streams have serious effects on the environment, and severe health problems for humans and animals. If the untreated contaminants such as heavy metals are released into environments, they are certain to cause significant environmental problems due to the accumulation in soil and water environments [1]. Environmental contamination by these heavy metals leads to non-biodegradability, bioaccumulation and toxicity even at lower concentrations [2–6]. Various methods have been developed for the removal of toxic

*Corresponding author.

heavy metals from an aqueous medium such as chemical precipitation, biological treatment, advanced oxidation process, electrochemical treatment, electrodialysis, membrane technology, ion exchange, and adsorption. Among the various treatment methods mentioned, the adsorption method is a viable alternative due to its high efficiency, low cost, easy operational conditions and effectiveness, even if heavy metals are present at low concentrations [7–13]. Carbon nanotubes, activated carbon, mesoporous carbon, coconut shell, fly ash, peanut shell and polymeric resins [14–17] suffer from low adsorption capacities and present difficulties in reuse. Therefore, efforts are in progress to develop new and highly efficient adsorbents.

Graphene is atomically thick graphite; it has concerned intensive two-dimensional sheet composed of sp^2 hybridized carbon atoms arranged in a honeycomb structure. Graphene has unique physical properties, such as an excellent thermal property, high intrinsic carrier mobility, mechanical strength, elasticity, and good electrical conductivity. In recent years, much research on graphene and graphene oxide (GO) has resulted in various applications in the field of material science, such as nanoelectronics, photocatalysis, batteries, sensors, super capacitors, transistors, flexible displays, touch screens, solar cells and composite materials [18,19]. Recently, graphene-based adsorption technology has been developed because of its high surface area and its perfect match with sp^2 hybridized structure, compared to carbon nanotubes and their carbon additives [20–24].

Magnetic nanoparticles have drawn significant interest and have been widely used in various promising applications, such as catalysis, electronic devices, information storage, sensors, drug-delivery technology, biomedicine, magnetic recording devices and environmental remediation [25–27]. Recently, Shahriari et al. used iron oxide magnetic nanoparticle in adsorption of chromium (III), while Elwakeel removed arsenate through adsorption using magnetic chitosan resin [28,29].

Graphene and Fe_3O_4 nanoparticles have been separately used for a variety of applications in the last few years, but the recent technological improvements and the resulting combination of graphene with Fe_3O_4 nanoparticles produces a magnetic graphene/Fe_3O_4 composite (GFC) with greater advantages and tremendous potential for applications [30,31]. In recent years, the exclusive properties of GFC have been exploited for extensive applications. For example, Narayanan et al. [32] studied the multifunctional preparation of reduced GO/Fe_3O_4 isolated membranes and their temperature-reliant electronic transport properties. Zhou et al. [33] have explored the application of graphene–Fe_3O_4 composites as biosensors. Yang et al. [34] have carried out studies on graphene–Fe3O4 nanoparticles for targeted drug delivery. In recent years, the GFC has been used as an adsorbent to remove toxic pollutants from an aqueous environment [35–37]. This GFC has certain advantages over conventionally used adsorbents, in terms of convenient magnetic separation, fast adsorption rate and elevated adsorption capacity.

In the present study, the synthesis of the GFC by the simultaneous GO reduction and conversion of $FeCl_3.6H_2O$ to Fe_3O_4 by a one-step solvothermal method has been carried out. The adsorption capacities of these adsorbents have been compared with those of other adsorbents. The effects of the pH, GFC dosage, contact time, metal ion concentration and temperature on adsorption have also been studied to determine the optimal conditions for Zn(II) and Ni(II) ions removal. Adsorption isotherms, the kinetics and thermodynamics of metal ion adsorption on the GFC have also been studied. Since the GFC has a magnetic property, it is separated from the adsorbate solution using a magnet.

2. Materials and methods

2.1. Materials

Graphite powder (98% purity), sulphuric acid, potassium permanganate, sodium nitrate, hydrogen peroxide, barium nitrate, ethylene glycol, ferric chloride hexahydrate, sodium acetate, polyethylene glycol, zinc sulphate, nickel sulphate, hydrochloric acid, sodium hydroxide and ethanol were purchased from SRL (Sisco Research Laboratories Pvt. Ltd.), and are of an analytical grade (98% purity).

2.2. Preparation of GO

GO was synthesized from natural graphite powder by Hummer's method [38,39]. In a typical procedure, graphite powder (2 g) was mixed with concentrated sulphuric acid (46 mL) and taken in a 250 mL double-necked round-bottomed flask, and 1 g of sodium nitrate was slowly added followed by stirring of the contents kept in an ice bath (20˚C). Then the reaction mixture was warmed to 35˚C and stirred for 30 min. After 30 min, deionized water (92 mL) was slowly added, which leads to an increase in temperature to an extent of 98˚C. External heating was then introduced to maintain the reaction temperature at 98˚C for 15 min and cooled using a water bath. Then, 280 mL of water was added to the

mixture followed by the addition of 30% hydrogen peroxide (2 mL). After air cooling at room temperature (28 ± 2˚C), the mixture was separated by filtration, multiple washing and centrifugation. The GO was purified by repeated centrifugation and redispersing in deionized water until a negative test for sulphate ion (with Ba $(NO_3)_2$) was achieved. The GO slurry was then dried in a vacuum oven at 60˚C for 48 h before being used.

2.3. Preparation of GFC

In a typical synthesis [40], the prepared GO (0.2 g) was mixed with 100 mL of ethylene glycol and dispersed by means of ultrasonication for 75 min. The dispersed GO solution was transferred into a 500 mL three-necked round-bottomed flask, and 1 g of $Fecl_3{\cdot}6H_2O$ was dissolved in the solution and mechanically stirred for 3 h. Then, 7.2 g of sodium acetate and 2 g of polyethylene glycol were added followed by stirring for another 30 min. Then the mixture was transferred into a 250 mL stainless-steel autoclave and kept at 200˚C for 12 h. A black colour product was obtained, washed with ethanol several times and dried in a vacuum oven at 60˚C for 6 h and used for further characterization.

2.4. Adsorbate

Stock solutions of 500 mg L^{-1} of Nickel (II) and Zinc (II) ions were prepared from $NiSO_4{\cdot}6H_2O$ and $ZnSO_4{\cdot}6H_2O$, respectively, using deionized water. Batch adsorption studies were performed using the diluted stock solutions. The pH of each test solution was adjusted to the desired pH, using 0.1 M NaOH or 0.1 M HCl before mixing with the adsorbent.

2.5. Analysis method

The solution pH was measured with a Hanna pH meter using a combined glass electrode. The Fourier transform infrared spectrometric analysis was carried out with KBr pellets using Bruker (Tensor 27) in the spectral range of 450–4,000 cm^{-1}. The Confocal Raman microscopic analysis was carried out in a CRM Alpha 300 WITec Raman spectrometer using 532 nm laser as the light source. X-ray powder diffraction (XRD) patterns were recorded using the Rigaku X-ray Diffractometer (miniflex II-C) with Cu Kα (λ = 0.154 nm) radiation operating at 35 kV and 25 mA in 2θ range of 20–80˚, with a step of 0.01˚ and integration time of 1 s. The morphology of the GO and GFC was observed by field emission scanning electron microscopy, and an elemental analysis was carried out using Quanta 3D FEG with energy dispersive analysis of X-ray (EDAX). The thermo gravimetric analysis (TGA) was performed for the GFC using TGA Q50 V20.10 build 36 analyzer (Shimadzu Japan). The magnetization properties were measured at room temperature on a vibrating sample magnetometer EG&G VSM Model 155 (VSM). The initial metal ion concentration before and after adsorption were determined by the AA6300 atomic absorption spectrometer (Shimadzu Japan).

2.6. Batch adsorption studies

Batch adsorption experiments were carried out by varying parameters like the pH (3–11), adsorbent dosage (5–25 mg), initial metal ion concentration (10–60 mg L^{-1}), contact time (0–90 min) and temperature (303–343 K). The adsorption experiments were carried out in a 250 mL conical flask, with a rotation speed of 200 rpm for a constant period of time using the horizontal bench shaker. At predetermined time intervals, the samples were withdrawn from the shaker and the adsorbent was removed from the contents solution using a magnet, and the concentration of metal ion in the solution was analysed using the AAS. The percentage removal of heavy metal ions was calculated using the mass balance equation,

$$\text{Metal ion percentage removal} = \frac{C_0 - C_e}{C_0} \times 100 \quad (1)$$

where C_0 and C_e are the initial and equilibrium concentrations of the metal ion (mg L^{-1}). The amount of heavy metal ion adsorbed per unit mass of the adsorbent was evaluated using the mass balance equation,

$$q_e = \frac{C_0 - C_e}{m} \times V \quad (2)$$

where V is the volume of the metal ion solution, (m) is the mass of the adsorbent, C_0 and C_e are the initial and equilibrium concentrations of the metal ion solution (mg L^{-1}), and q_e is the amount of metal ion adsorbed (mg g^{-1}) per gram of the adsorbent.

2.7. GFC recycle study

To evaluate the reversibility and regeneration of adsorbents, the metal ions (Zn(II) and Ni(II) ions)

adsorbed adsorbent (GFC) was mechanically stirred at room temperature with 25 ml of 0.1 N HCl for 5 h in order to desorp Zn(II) and Ni(II) ions from the GFC. The solution pH was maintained at 5.5. The adsorbent was separated from the content using a magnet, washed with DI water, filtered and then dried at 60°C for 3 h [41–43]. The desorption of metal ions was confirmed by AAS examination. The recovered GFC was used for further adsorption studies and was evident that the recycling can be repeated for four times. The adsorption capacity of this adsorbent, remaining almost the same with reuse, makes it a good choice for multicyclic use.

3. Results and discussion

3.1. Characterization of the GFC

3.1.1. FTIR spectroscopy

FTIR spectroscopy is a useful tool for the detection of functional groups present on a nanoparticle surface. The FTIR spectra of GO and GFC are shown in Fig. 1(a) and (b), respectively. From Fig. 1(b), it can be seen that the peaks at 1,727 cm^{-1} (C=O group) and 1,616 cm^{-1} (O–H groups) are absent in confirmation to Fig. 1(a), which evidences the reduction of GO to graphene. New absorption peaks appearing at 1,566 and 2,902 cm^{-1} in GFC may be attributed to the skeletal vibrations of the graphene sheets and to the asymmetric CH_2 stretch in the composite. The peak at 576 cm^{-1} corresponds to the vibration of FeO, which clearly indicates the GFC formation.

3.1.2. Raman spectroscopy

Raman spectroscopy helps to distinguish materials in different structural phases. Raman spectra were recorded for the GO and GFC, and are shown in Fig. 2(a) and (b). It can be seen that the D band in both GO and GFC appears at 1,351 cm^{-1} with a varied intensity. The increase in intensity of the D band in the composite may be attributed to the introduction of a defect during the reduction of GO. The G band appears at 1,592 cm^{-1} in the case of GO and at 1,572 cm^{-1} in the case of GFC, of course with different intensities. The change in position and variation in intensity may be due to the stress originated during the composite formation. The I_D/I_G ratio of the GFC was found to be higher than that of the initial GO.

3.1.3. XRD analysis

XRD patterns were studied for GO and GFC, as shown in Fig. 3(a) and (b). In the case of GO in Fig. 3(a), the peak at $2\theta = 10.88^\circ$ corresponds to the oxygen functionality (0 0 1), which was absent in the GFC; the disappearance of this peak also evidences the reduction of GO. The Fe_3O_4 (1 1 1) peak at $2\theta = 35.36^\circ$ in the GFC shows its incorporation into graphene (0 0 2). From Fig. 3(b) in GFC, a small peak can be seen at $2\theta = 24^\circ$, which further evidences the formation of the GFC. The incorporation of Zn(II) and Ni(II) ions onto GFC can be clearly seen from the XRD patterns, as shown in Fig. 4(a) and (b), respectively. The peaks at $2\theta = 20$–240 in Fig. 4(a) and (b) corresponds to Zn(II) and Ni(II) ions adsorption onto GFC.

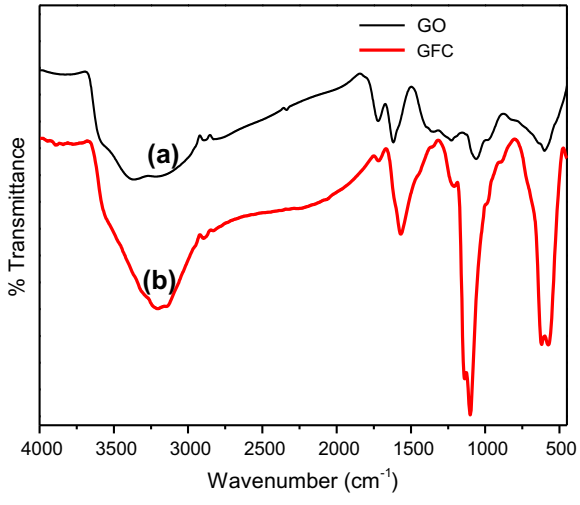

Fig. 1. FT-IR spectrum of (a) GO and (b) GFC.

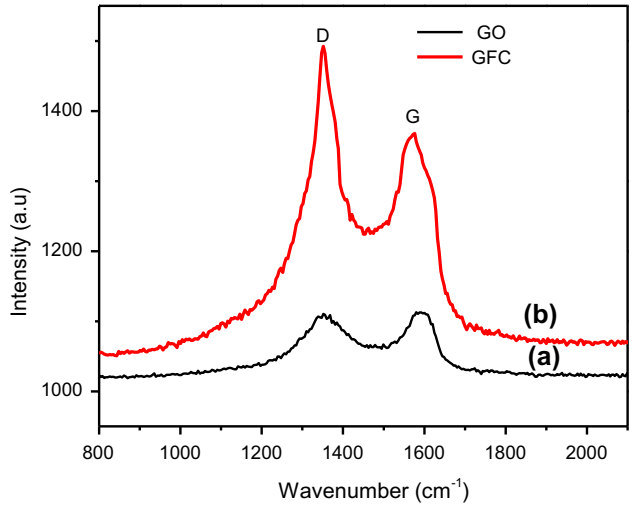

Fig. 2. Raman spectra of (a) GO and (b) GFC.

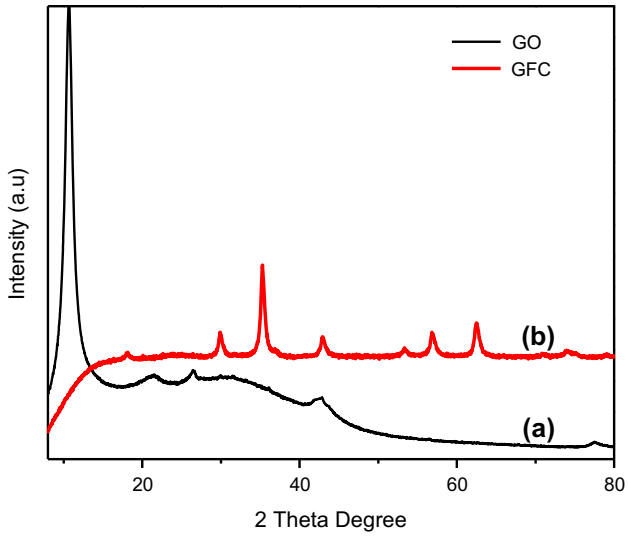

Fig. 3. XRD patterns of (a) GO and (b) GFC.

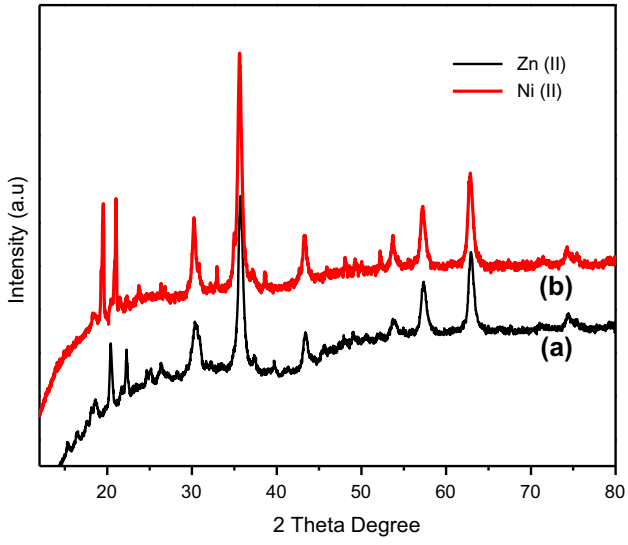

Fig. 4. XRD patterns of (a) Zn(II) and (b) Ni(II) ions adsorption onto the GFC.

3.1.4. SEM and EDAX analysis

The scanning electron microscope (SEM) analysis is helpful for surface morphological studies. All the SEM images shown are of 400 nm size. It can be seen from Fig. 5(a) that the GO has a thick sheet like structure and a smooth surface. The surface morphology of the GO subjected to a single-step solvothermal process, in which simultaneous reduction of the GO and incorporation of Fe_3O_4 takes place, is shown in Fig. 5(b). The appearance of spherical bead-like Fe_3O_4 on the smooth layer of graphene can be seen from Fig. 5(b), which was attributed to an increase in the surface area. The increase in the surface area helps the adsorption of a large amount of Zn(II) and Ni(II) ions, which could be seen from the SEM images of Zn(II) and Ni(II) ions adsorbed on GFC as shown in Fig. 5(c) and (d).

The EDAX analyses of GO, GFC, Zn(II) adsorbed GFC and Ni(II) adsorbed GFC were carried out, and are shown in Fig. 6(a)–(d). Fig. 6(a) shows peaks corresponding to C and O, which are characteristic of GO. In Fig. 6(b), peaks corresponding to Fe are also seen in addition to the C peaks and the peaks corresponding to O vanish, which proves the reduction of GO to graphene and the formation of the GFC. In Fig. 6(c) and (d), the peaks corresponding to the Zn(II) and Ni (II) ions can be clearly seen in addition to the C and Fe, which evidences the adsorption of Zn(II) and Ni(II) ions onto the GFC.

3.1.5. TGA analysis

The thermal properties of the GFC composite have been studied by the TGA conducted at a particular temperature range (room temperature to 700˚C), in air atmosphere, with a heating range of 10˚C min^{-1}. As observed from Fig. 7, the weight loss at nearly 120˚C was attributed to the evaporation of the adsorbed solvent. The GFC composite was found to undergo a gradual weight loss between 120 and 400˚C, because of oxidation and decomposition. From the TGA curve, it can be inferred that the weight loss of GFC was below 24%, which evidences the presence of graphene.

3.1.6. VSM analysis

The investigation of the magnetic properties of the GFC was carried out with an applied magnetic field (15 kOe) at room temperature, using a VSM. From Fig. 8, it can be seen that the magnetic hysteretic loops of the GFC have a saturation magnetization of 37.19 emu, and exhibit a superparamagnetic character. The saturation magnetization value of the GFC was found to be lower than that of pure Fe_3O_4, which indicates the existence of graphene in the composite.

3.2. Effect of operating parameters

3.2.1. Effect of pH

The pH of the aqueous solution is an important factor that may influence the uptake by the adsorbent, in which the chemical characteristics of both adsorbent and adsorbate will vary with the pH [44]. Adsorption

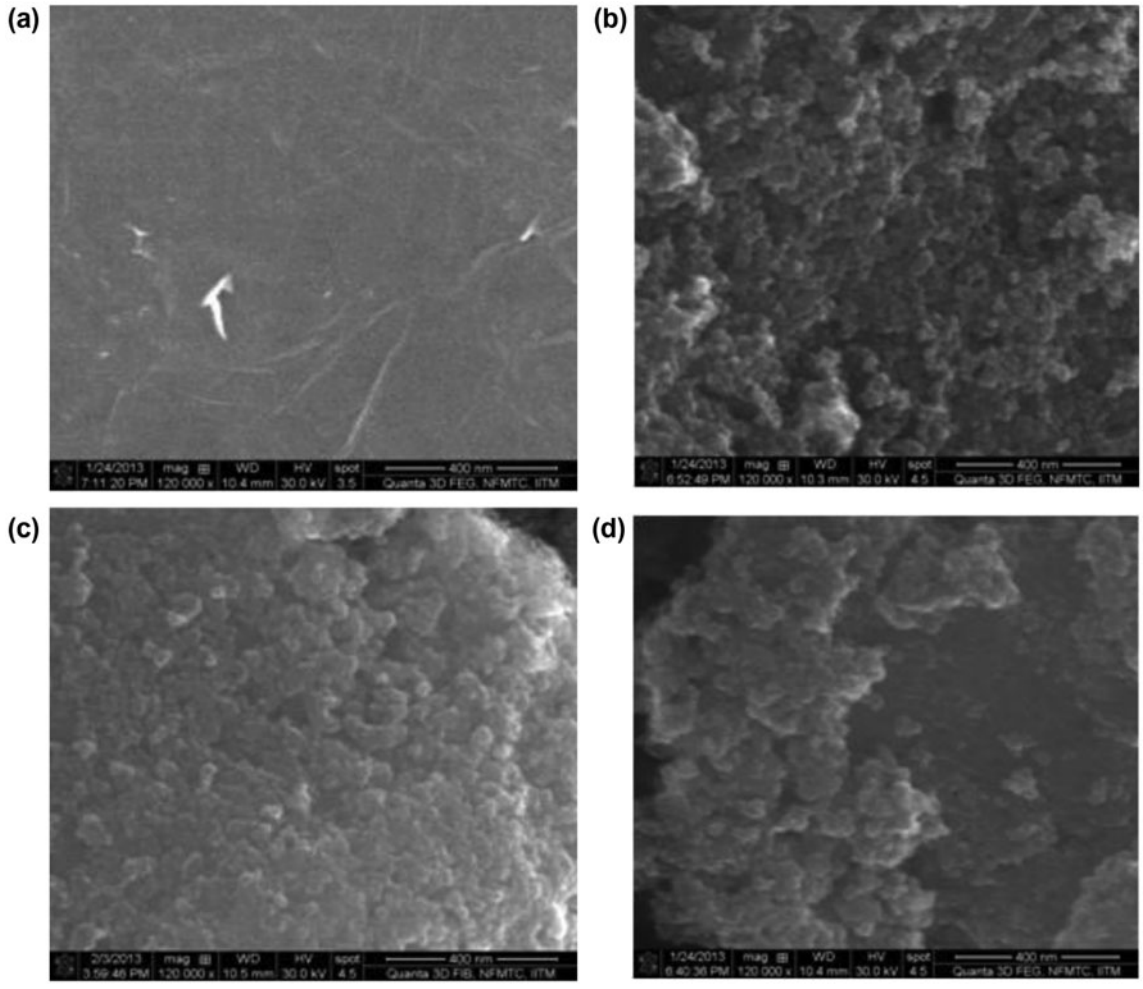

Fig. 5. SEM images of (a) GO, (b) GFC, (c) Zn(II), and (d) Ni(II) ions adsorption onto the GFC.

studies were carried out in the pH range of 3–11 with the GFC. The adsorption increases with an increase in the pH up to a value of 7, as shown in Fig. 9(a). Beyond pH 7, the percentage removal decreases; this may be due to the precipitation of the metal ions as their hydroxides. At a lower pH, the competition of H^+ ions for active sites in the adsorbent leads to a lesser percent removal of the metal ions. Hence pH 7 was found to be the optimum, and this pH was used for further studies.

3.2.2. Effect of the GFC dosage

Fig. 9(b) shows the effect of the GFC dosage on batch adsorption. Batch adsorption studies were carried out with GFC varied in the range of 0.1–0.5 g L^{-1}. The metal ion solution concentration was 30 mg L^{-1}, equilibrium time was 60 min, pH 7 and the contents were agitated at 200 rpm for the adsorption experiments. The increase in GFC dosage appeared to promote more active sites, which facilitated the adsorption of pollutants [45]. It can be seen that the percentage removal increases up to 0.3 g L^{-1}, beyond which there was no significant increase due to the saturation of the active sites.

3.2.3. Effect of metal ion concentration

The effect of the metal ion concentration over adsorption in the GFC, with different initial metal ion concentrations (10–60 mg L^{-1}) was studied at pH 7; the GFC dosage was fixed as 0.3 g L^{-1}, equilibrium time 60 min, temperature 303 K and the results obtained are given in Fig. 9(c). The metal ion removal decreases with increasing metal ion concentration, because the active adsorption sites are completely filled with the metal ions.

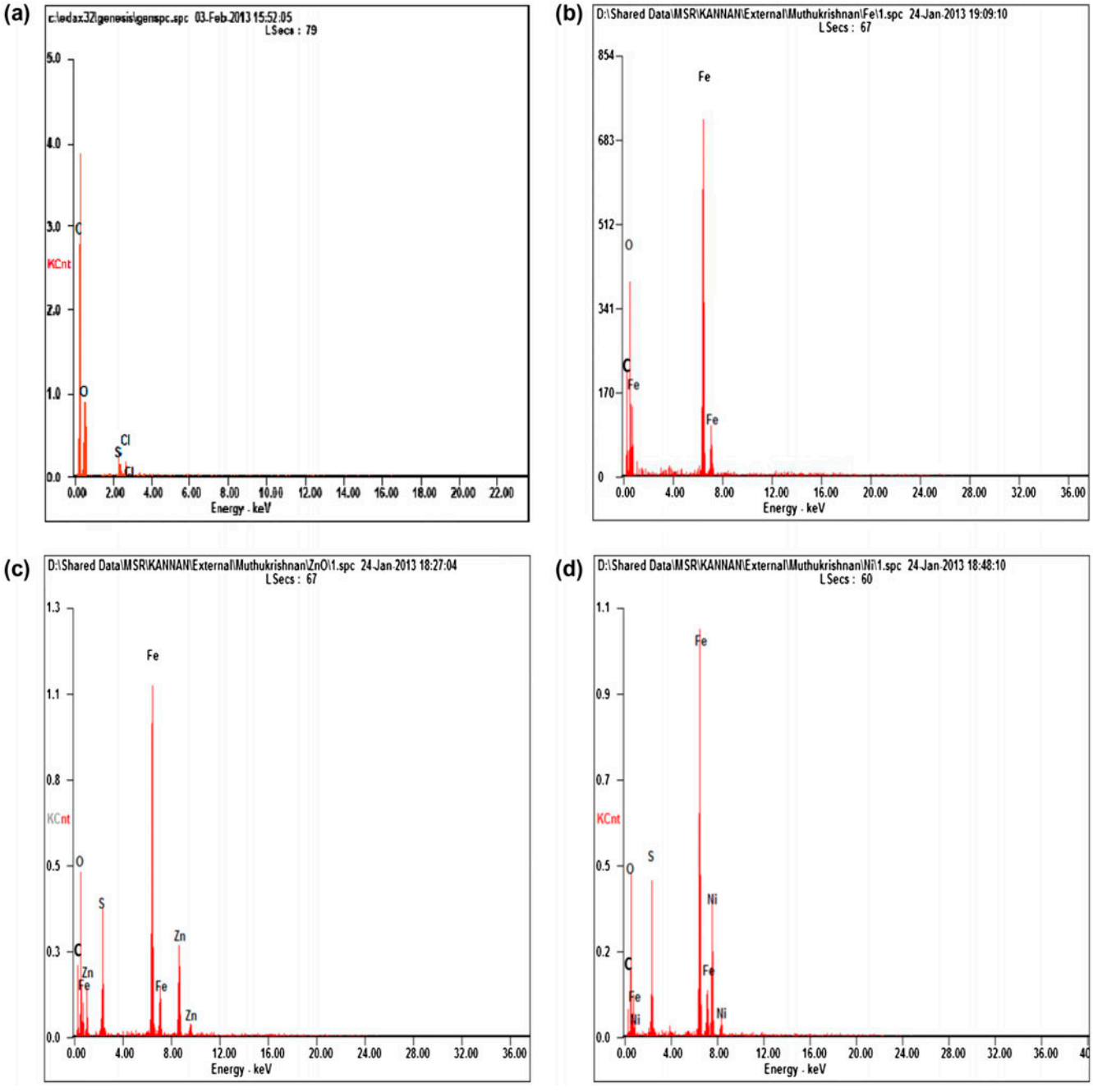

Fig. 6. EDAX spectra of (a) GO, (b) GFC, (c) Zn(II), and (d) Ni(II) ions adsorption onto the GFC.

3.2.4. Effect of contact time

The adsorption efficiency increases with an increase in the contact time gradually from 10 to 60 min, beyond which there was no significant increase, as shown in Fig. 9(d). During the initial steps, the removal was high because of the availability of more number of active sites. After the attainment of equilibrium, the active sites are occupied by the metal ions.

3.2.5. Effect of temperature

Fig. 9(e) shows the effect of temperature on the adsorption of metal ions onto the GFC. Temperature studies were carried out with an adsorbent dose of 0.3 g L^{-1}, time of 60 min, metal ion concentration of 30 mg L^{-1} and in the temperature range of 303–343 K. With an increase in temperature from 303 to 343 K, the metal ion removal increases slightly which shows

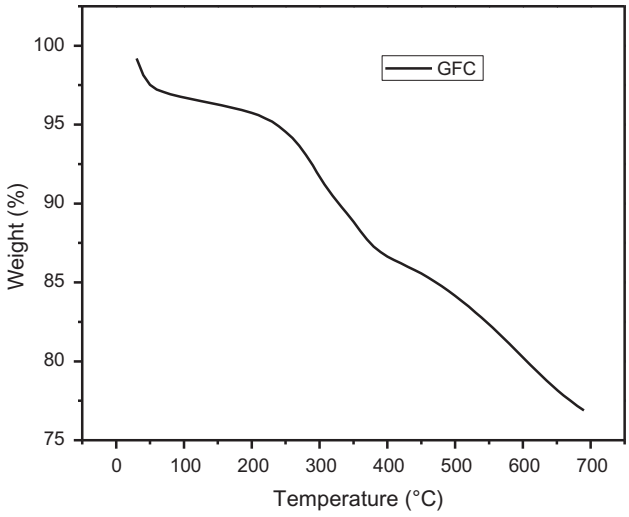

Fig. 7. TGA curve of GFC.

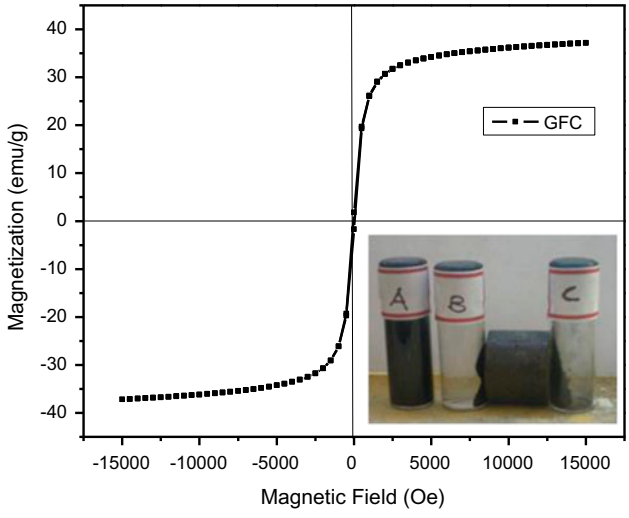

Fig. 8. Room temperature magnetization behavior of GFC.

that the adsorption was endothermic. With an increase in the temperature, the interaction between the solute and the adsorbent was higher than that between the solute and the solvent.

3.3. Isotherm studies

Adsorption isotherm models explain the distribution of molecules between the liquid and solid phases, when the adsorption process attains the equilibrium state. The analysis of the isotherm data by fitting them to different isotherm models is an important step in finding a suitable model that can be used for design purposes. The non-linear forms of Langmuir [46], Freundlich [47], Redlich–Peterson [48], Temkin and Pyzhev [49] were used to evaluate the adsorption experimental data using MATLAB R2011a.

3.3.1. Langmuir isotherm model

The Langmuir isotherm is probably the best known and most widely used adsorption isotherm. This is based on the assumption that maximum adsorption occurs when a saturated monolayer of the solute molecules was present on the adsorbent surface; the energy remains constant and there was no migration of the adsorbate molecules in the surface plane. The non-linear equation of the Langmuir model is expressed as follows:

$$q_e = \frac{q_m K_L C_e}{1 + K_L C_e} \tag{3}$$

where C_e is the equilibrium concentration of the metal ions in the solution (mg L^{-1}), q_e is the adsorbed value of the metal ion at an equilibrium concentration (mg g^{-1}), q_m is the maximum adsorption capacity (mg g^{-1}) and K_L is the Langmuir binding constant related to the energy of adsorption.

The essential characteristics of the Langmuir isotherm parameters can be used to explain the attraction between the adsorbate and adsorbent using the dimensionless constant, R_L (separation factor), expressed as

$$R_L = \frac{1}{1 + K_L C_0} \tag{4}$$

where K_L is the Langmuir constant and C_0 is the initial concentration of Zn(II) and Ni(II) ions. The R_L value plays a vital role in predicting the nature of adsorption. The R_L value of zero implies that the isotherm was irreversible, favourable when $0 < R_L < 1$, linear when $R_L = 1$ linear and unfavourable when $R_L > 1$. The Langmuir isotherm parameters are given in Table 1.

3.3.2. Freundlich isotherm model

The Freundlich isotherm is related to multilayer adsorption on a heterogeneous surface and the application of the Freundlich equation suggests that the adsorption energy decreases exponentially on the saturation of the adsorption centres sites in an adsorbent. The non-linear form of the Freundlich model is given by the following equation:

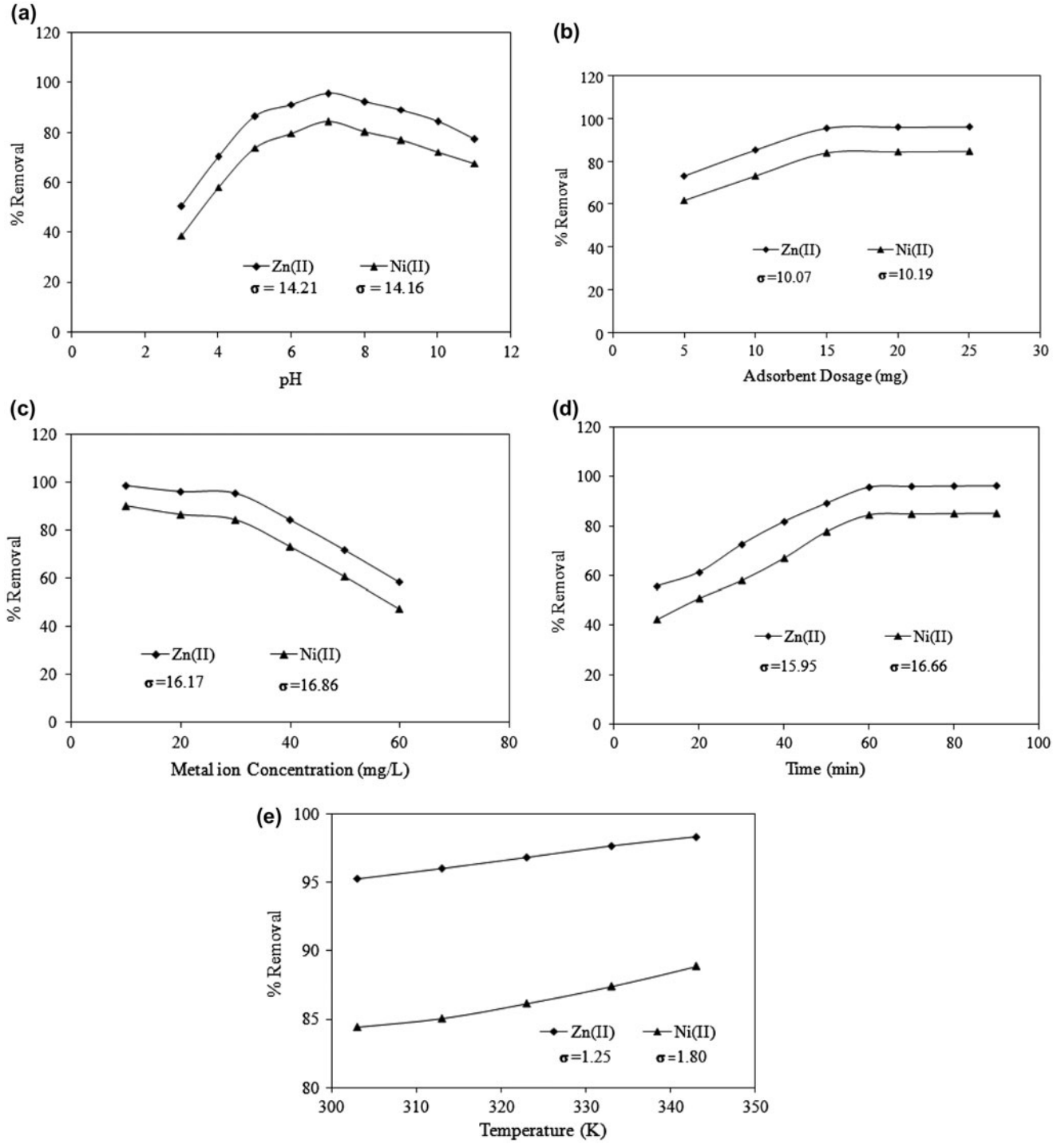

Fig. 9. (a) Effect of pH for the adsorption of metal ions onto GFC (the initial metal ion concentration 30 mg L^{-1}, GFC dosage = 0.3 (g L^{-1}) time = 60 min, and temperature = 303 K), (b) effect of adsorbent dosage (GFC) on metal ion removal (the initial metal ion concentration 30 mg L^{-1}, pH 7, time = 60 min, and temperature = 303 K), (c) effect of metal ion concentrations for the adsorption of metal ions onto GFC (the initial metal ion concentration 10–60 mg L^{-1}, pH 7, GFC dosage = 0.3 (g L^{-1}) time = 60 min, and temperature = 303 K), (d) effect of contact time for the adsorption of metal ions onto GFC (the initial metal ion concentration 30 mg L^{-1}, pH 7, GFC dosage = 0.3 (g L^{-1}), time = 10–90 min, and temperature = 303 K), and (e) effect of temperature on the adsorption of metal ions onto GFC (the initial metal ion concentration 30 mg L^{-1}, pH 7, GFC dosage = 0.3 (g L^{-1}), time = 60 min, and temperature = 303–343 K).

Table 1
The value of parameters for all isotherm models used in this present study

Isotherm model	Parameters Zn(II) ion	R^2	Parameters Ni(II) ion	R^2
Langmuir	k = 1.949	0.971	k = 0.4567	0.9659
	q = 121.5		q = 111.4	
Freundlich	k = 72.02	0.8415	k = 47.03	0.8146
	n = 5.484		n = 4.039	
Temkin	a = 72.74	0.9153	a = 6.611	0.8961
	b = 7.425		b = 8.948	
Redlich–Peterson	α_R = 2.07	0.9711	a = 2	0.8902
	β = 0.9924		b = 0.845	
	K_R = 4.245		k = 8.115	
	q = 57.98		q = 15.94	

$$q_e = K_f C_e^{\frac{1}{n}} \tag{5}$$

where K_f is the Freundlich constant ((mg g^{-1}) (L mg^{-1})$^{1/2}$) that indicates the adsorption capacity and represents the strength of the adsorption band, and "n" is the heterogeneity factor that represents the bond distribution. The value of "n" explains the degree of non-linearity between the solution concentration and adsorption as follows: if $n = 1$, adsorption is linear; if $n < 1$, adsorption is a chemical process and if $n > 1$, then adsorption is a physical process. The values of "n" obtained were between 1 and 10, which indicates the physical adsorption of Zn(II) and Ni(II) ions onto the GFC. All other parameters are listed in Table 1.

3.3.3. Temkin isotherm model

The Temkin isotherm describes the behaviour of adsorption on a heterogeneous surface. The derivation of the Temkin isotherm assumes that the fall in the heat of adsorption is linear rather than logarithmic, as implied by the Freundlich equation. The Temkin isotherm is expressed as follows:

$$q_e = B \ln (AC_e) \tag{6}$$

where $B = RT/b$, "b" is the Temkin constant related to the heat of adsorption (J mol^{-1}), "A" is the Temkin isotherm constant (L g^{-1}), "R" is the universal gas constant (8.314 J mol^{-1} K^{-1}) and "T" is the absolute temperature (K). R^2 and the Temkin constant values are presented in Table 1.

3.3.4. Redlich–Peterson isotherm model

The Redlich–Peterson isotherm is a combination of the Langmuir and Freundlich models. This model is used to evaluate the homogeneous and heterogeneous nature of Zn(II) and Ni(II) ions adsorption onto the GFC. The non-linear Redlich–Peterson isotherm model equation is given by:

$$q_e = \frac{K_R C_e}{1 + \alpha_R C_e^{\beta}} \tag{7}$$

where K_R (L g^{-1}) and α_R (L mg^{-1}) are the Redlich–Peterson constants, and β is the Redlich–Peterson exponent which lies between 0 and 1. If the β value = 1, the adsorption follows the Langmuir model; if $\beta = 0$, it follows the Henry isotherm model. The experimental data were fitted to the non-linear Redlich–Peterson isotherm model; the parameters were calculated and are listed in Table 1.

Based on the R^2 value, the experimental isotherm data were fitted (Zn(II) and Ni(II)) in the order of the Langmuir > Redlich–Peterson > Temkin > Freundlich isotherm models, and the graphical representation of these models are given in Fig. 10(a) and (b). The Langmuir isotherm is explained by the formation of a homogeneous monolayer. The monolayer was formed by the π–π interaction between the positively charged metal ion and the aromatic regions. It was also supported by the β value in the Redlich–Peterson isotherm, where β was close to 1. A comparison of maximum monolayer adsorption capacity of Zn(II) and Ni(II) onto various adsorbents is listed in Table 2.

The schematic representation for the metal ions on to the GFC is given in Fig. 11. The experimental isotherm data were also fitted with the Temkin and Freundlich isotherm models, which show the heterogeneous multilayer surface on the GFC. The heterogeneous surfaces present in the GFC are the –COOH and –OH groups. The metal ions are adsorbed by the π–π interaction of the metal ions and the functional groups present in the GFC.

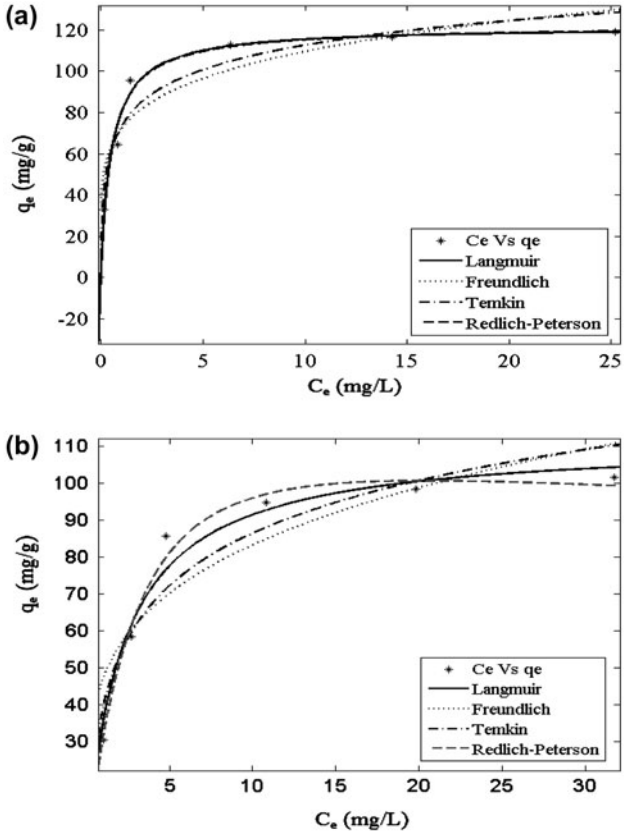

Fig. 10. (a) Non-linear adsorption isotherm for Zn(II) ions with GFC and (b) non-linear adsorption isotherm for Ni(II) ions with GFC.

3.4. Adsorption kinetics

Adsorption kinetic studies have been used to predict the controlling mechanism of the adsorption process. Various kinetic models, namely, the Lagergren pseudo-first-order model [50], Ho's pseudo-second-order model [51], Elovich [52], and Weber and Morris intraparticle diffusion kinetic [53] models have been applied to the present experimental data.

3.4.1. Lagergren pseudo-first-order kinetic model

Lagergren pseudo-first-order equation is given by:

$$\log(q_e - q_t) = \log q_e - \frac{K_{ad}}{2.303}t \tag{8}$$

where q_t is the adsorption capacity at time t (mg g^{-1}) and K_{ad} (1 min^{-1}) is the rate constant of the pseudo-first-order adsorption process. Fig. 12(a) shows that the slope and intercept of the plot of "log ($q_e - q_t$)" vs. "t" were used to determine the pseudo-first-order rate constant K_{ad}, and the equilibrium adsorption capacity q_e. The value of correlation coefficient (R^2) and all other parameters are outlined in Table 3.

3.4.2. Ho's pseudo-second-order kinetic model

Ho's pseudo-second-order kinetic equation is given by

$$\frac{t}{q_t} = \frac{1}{Kq^2} + \frac{1}{q_e}t \tag{9}$$

where K is the rate constant for the pseudo-second-order (gm g^{-1} min^{-1}) mechanism. Fig. 12(b) shows that the plot of "t/q_t" vs. "t" is linear, from which q_e and K were determined from the slope and intercept. All other data are presented in Table 3.

3.4.3. Elovich kinetic model

The Elovich kinetic model can be expressed as follows:

Table 2
Comparison of metal ion adsorption capacities of various adsorbents

Types of adsorbent	q_{max} (mg g^{-1})		References
	Zn(II)	Ni(II)	
Cork biomass	44.60	22.22	[55]
Wheat bran	–	12.00	[56]
Cone biomass of *T. orientalis*	–	12.42	[57]
Dye loaded sawdust	17.09	9.87	[58]
Irish peat moss	–	14.5	[59]
P-tert[(dimethylamino) methyl]-calix[4]arene	36.40	52.80	[60]
Modified coir fibers	7.88	4.33	[61]
Unmodified coir fibers	1.83	2.51	[61]
GFC	121.5	111.4	Present work

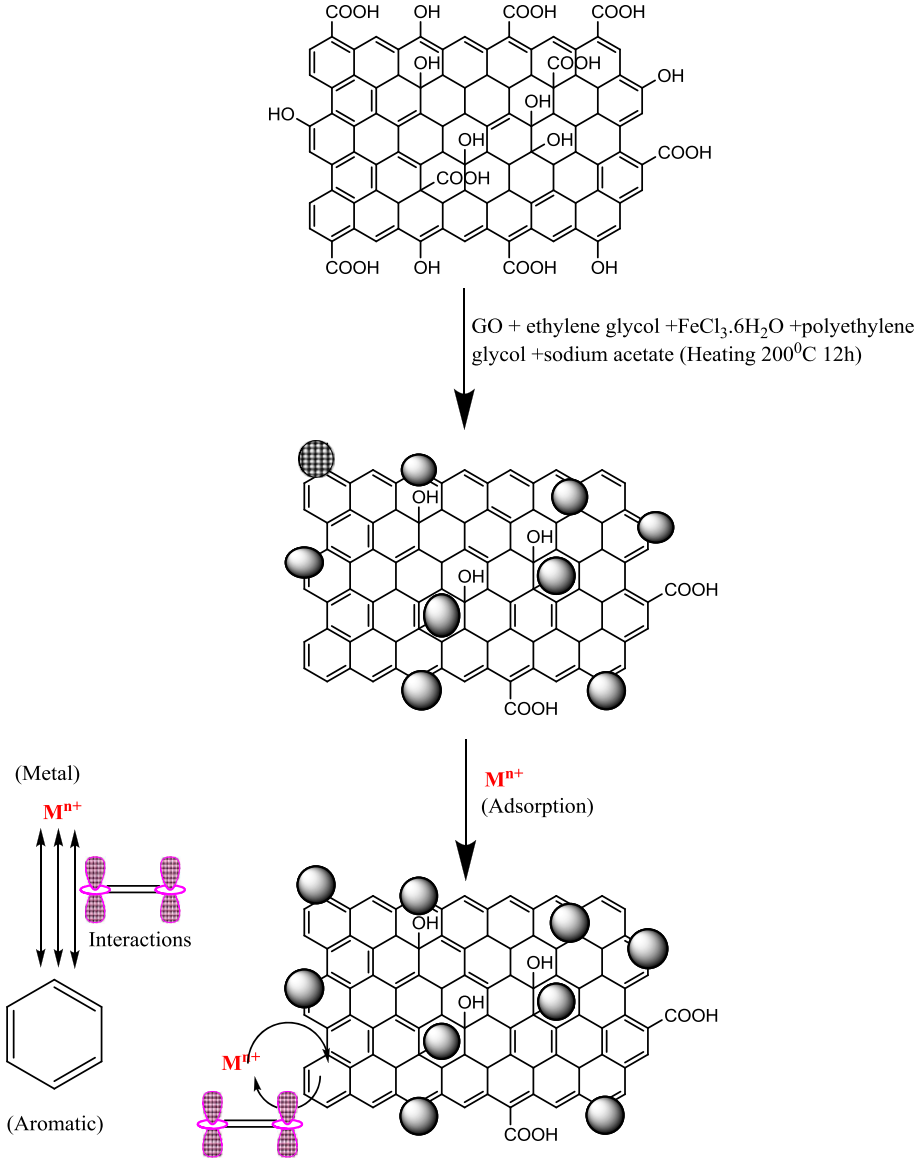

Fig. 11. The schematic representation for the metal ions removal on to GFC.

$$q_t = \frac{1}{\beta}\ln(\alpha\beta) + \frac{1}{\beta}\ln t \quad (10)$$

where α is the initial adsorption rate in (gm g^{-1}) and β (gm g^{-1}) is the desorption constant related to the extent of the surface coverage and activation energy for chemisorptions. The metal ion adsorption kinetics onto GFC was also tested with the Elovich kinetic model by plotting "q_t" vs. "ln (t)" as shown in Fig. 12(c). The α, β and R^2 values are listed in Table 3.

3.4.4. Weber and Morris intraparticle kinetic model

The Weber and Morris intraparticle kinetic model has been used to predict the influence of the mass transfer resistance on the binding of the metal ion onto the GFC. This model is expressed by the following equation:

$$q_t = K_p t^{\frac{1}{2}} + C \quad (11)$$

where K_p is the intraparticle diffusion rate constant (mg g^{-1} min^{-1}) and "t" is the time (1 min^{-1}). The value

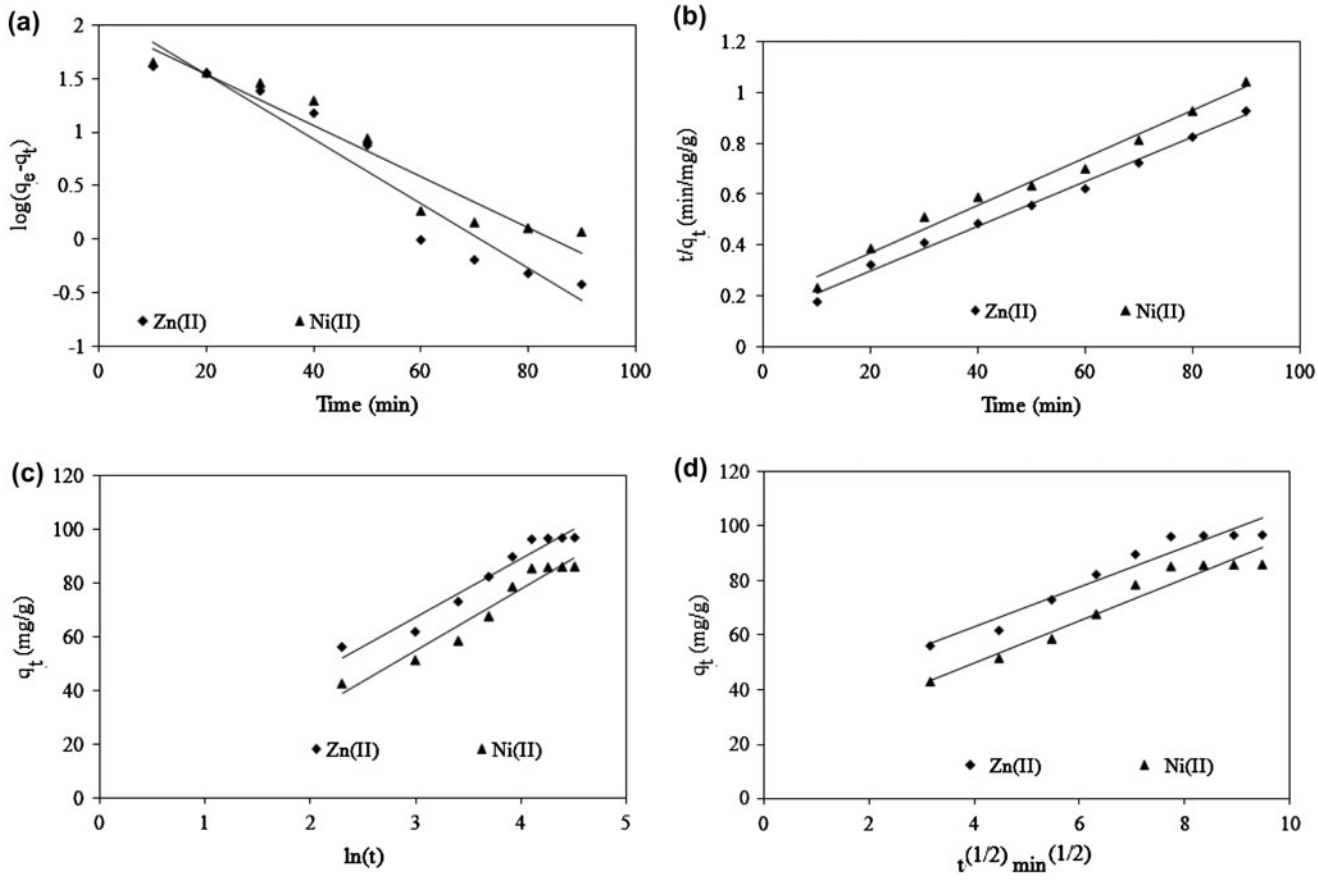

Fig. 12. (a) Pseudo-first-order kinetic model for adsorption of Zn(II) and Ni(II) ions onto GFC, (b) pseudo-second-order kinetic model for adsorption of Zn(II) and Ni(II) ions onto GFC, (c) Elovich kinetic model for adsorption of Zn(II) and Ni (II) ions onto GFC, and (d) intra-particle diffusion kinetic model for adsorption of Zn(II) and Ni(II) ions onto GFC.

Table 3
Kinetic models and other statistical parameters for Zn(II) and Ni(II) on to GFC under optimum conditions

Kinetic model	Parameters	Metal ion solutions	
		Zn(II)	Ni(II)
Pseudo-first-order kinetics	k_{ad} (1 min^{-1})	8.52×10^{-2}	5.98×10^{-2}
	$q_{e,cal}$ (mg g^{-1})	211.83	121.33
	R^2	0.942	0.924
Pseudo-second-order kinetics	k (g mg^{-1} min^{-1})	5.245×10^{-4}	4.378×10^{-4}
	$q_{e,exp}$ (mg g^{-1})	97.28	87.40
	$q_{e,cal}$ (mg g^{-1})	125	111.11
	h (mg g^{-1} min^{-1})	8.188	5.395
	R^2	0.992	0.983
Elovich model	α (mg g^{-1} min^{-1})	25.515	17.939
	β (g mg^{-1})	0.046	0.043
	R^2	0.950	0.948
Intra-particle diffusion model	k_p (mg g^{-1} $min^{1/2}$)	7.752	7.346
	β (g mg^{-1})	18.700	33.450
	R^2	0.943	0.937

of K_p and the constant (C) can be calculated from the slope and intercept of the linear plot of "q_t" vs. $t^{(1/2)}$, as shown in Fig. 12(d). The intercept of the plot gives the boundary layer effect. Larger the intercept, greater the contribution of the surface adsorption in the rate controlling step. The intraparticle diffusion straight line does not pass through the origin. This deviation from the origin is perhaps due to the difference in the rate of mass transfer in the initial and final stages of the adsorption. The calculated intraparticle rate constant and R^2 values are given in Table 3.

Table 3 suggests that the correlation coefficient R^2 value for the pseudo-second-order model was higher than that of the other kinetic models. The Elovich kinetic model does not give any proper mechanism, but has been found useful to describe the chemical adsorption on heterogeneous adsorbents. Moreover, the values of $q_{e(\mathrm{cal})}$ as obtained from the pseudo-second-order kinetic model are close to the $q_{e(\mathrm{exp})}$ values. These results prove that the adsorption data fit better with the pseudo-second-order kinetic model than with the intraparticle kinetic, the pseudo-first-order and the Elovich kinetic models, and hence, the rate limiting step of the metal ions onto the GFC in the present work. Hence, the pseudo-second-order kinetic model indicates that the adsorption depends on both the adsorbate and the adsorbent, which involves chemisorption in addition to physisorption. The attraction involved via sharing or exchange of electrons between the adsorbent and the adsorbate was due to the rate-limiting step involved in chemisorption.

3.5. Adsorption thermodynamic studies

Thermodynamic parameters are used to predict the feasibility and spontaneity of the process. Batch adsorption experiments were performed at different temperatures of 303, 313, 323, 333, and 343 K for an initial metal ion concentration of 30 mg L^{-1}, time 60 min and pH 7. The thermodynamic parameters such as change in standard enthalpy (ΔH°), Gibbs free energy (ΔG°), and entropy (ΔS°) of the adsorption can be calculated from the following equations:

$$\Delta G^\circ = \Delta H^\circ - T\Delta G^\circ \tag{12}$$

$$\log K_c = \frac{\Delta S^\circ}{2.303R} - \frac{\Delta H^\circ}{2.303RT} \tag{13}$$

where K_c is the equilibrium constant, C_e is the equilibrium concentration in solution, C_{Ae} is the amount of the metal ions adsorbed per litre of solution at equilibrium (mg g^{-1}) and T is the solution temperature in Kelvin. ΔH° and ΔS° were calculated from the slope and intercept of the Van't Hoff plots of "log K_c" vs. "$1/T$". This is shown in Fig. 13, and the results are listed in Table 4.

The value of ΔH° was positive which shows the endothermic nature of adsorption. The positive ΔS° value can be used to explain the increase in randomness at the solid/liquid interface during the adsorption of Zn(II) and Ni(II) ions onto the GFC. The negative value of ΔG° shows the highly feasible and spontaneous nature of the adsorption process. In addition, the higher negative value with an increase in temperature shows that the amount of metal ions adsorbed at equilibrium increases with an increase in the temperature, and heavy metal adsorption on GFC is an entropy-driving process [54]. The increase in % removal of metal ions at higher temperature may be due to the enlargement of the pore size and activation of the GFC surface.

3.6. Competitive adsorption of Zn(II) and Ni(II) ions

Competitive adsorption technique has received more attention nowadays, due to its simplicity and high efficiency in the removal of different metal ions from the aqueous solution. The competitive adsorption of Ni(II) and Zn(II) ions onto GFC was carried out with the mixture of the respective metal ion solutions, each with an initial concentration of 50 mg L^{-1} at optimum pH 7 for 60 min. The selectivity adsorption behaviour of these metal ions was different, and the percentage removal of Zn(II) and Ni(II) ions onto the GFC decreased in the mixture of zinc and nickel solution, compared to that of non-competitive adsorption. In the competitive adsorption process, the percentage removal of Zn(II) ions was greater than that of the Ni

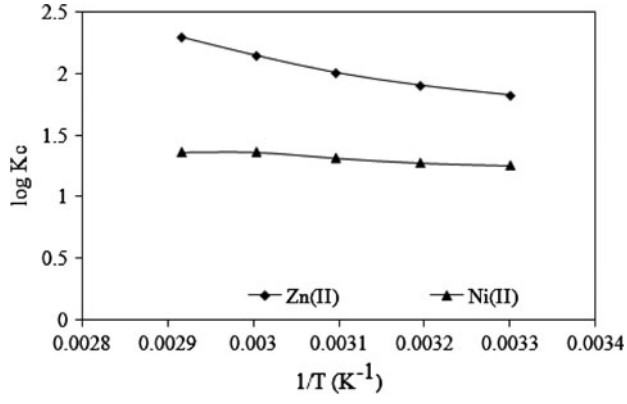

Fig. 13. Thermodynamic study (Plot of log K vs. $1/T$) for adsorption of Zn(II) and Ni(II) ions onto GFC.

Table 4
Thermodynamic parameters for the adsorption of Zn(II) and Ni(II) ions onto GFC

Parameter	Temperature (K)	Metal ion solutions	
		Zn(II)	Ni(II)
ΔH° (kJ mol^{-1})		23.282	6.006
ΔS° (J mol^{-1})		111.130	43.800
$-\Delta G^{\circ}$ (kJ mol^{-1})	303	10.353	7.265
	313	11.460	7.703
	323	12.573	8.141
	333	13.680	8.579
	343	14.793	9.010

(II) ions, but both ions can be removed in a single step. The removal order of the different metal ions studied (Zn 133 and Ni 124 pm) depends on the atomic radii of metal ions (Zn > Ni). The smaller atomic radius of the metal ions was the easier in diffusion on the adsorption site, and hence, the percentage removal from the surface was higher. The adsorption selectivity results show that the GFC adsorbent has good adsorption selectivity, easily recyclability, high adsorption capacity and cost effective for the removal various metal ions.

4. Conclusions

In this work, the facile one-step solvothermal synthesis of GFC adsorbent has been done followed by its characterization and adsorption, demonstrated with the removal of Zn(II) and Ni(II) ions from an aqueous environment. This GFC was obtained by the *in situ* reduction of $FeCl_3{\cdot}6H_2O$ to Fe_3O_4, and simultaneous conversion of GO to graphene in the presence of ethylene glycol and sodium acetate. The GFC formation was confirmed by the XRD, Raman and FTIR analysis. The maximum percentage removal of Zn(II) and Ni(II) ions are 96 and 87%, respectively, onto the GFC, achieved under pH 7, adsorbent dosage 0.3 g L^{-1}, metal ion concentration 30 mg L^{-1}, time 60 (min) and temperature 303 K conditions. Batch adsorption studies have been performed for isotherm, kinetics and thermodynamic studies. The adsorption isotherm data were well fitted to the Langmuir model due to its high correlation coefficient, and the maximum adsorption capacities of the GFC adsorbent towards Zn(II) and Ni (II) ions are 121.5 and 111.4 mg g^{-1}, respectively. The kinetic studies showed that the pseudo-second-order model was well described in the adsorption process. The thermodynamic studies show (303–343 K) that Zn (II) and Ni(II) ions adsorption onto GFC were spontaneous and endothermic in nature. Compared to other adsorbents, the GFC was easily recoverable, recyclable and has good adsorption efficiency in the removal of heavy metals from industrial effluents. The GFC has been reused a minimum of four times, with a slight decrease in the adsorption capacity.

References

[1] T.Y. Wu, G. Ningqun, Y.T. Chee, X.W.H. Jacqueline, Advances in Ultrasound Technology for Environmental Remediation, Springer, Netherlands, 2013, doi: 10.1007/978-94-007-5533-8.
[2] S. Sthiannopkao, S. Sreesai, Utilization of pulp and paper industrial wastes to remove heavy metals from metal finishing wastewater, J. Environ. Manage. 90 (2009) 3283–3289.
[3] T.K. Sen, S.P. Mahajan, K.C. Khilar, Adsorption of Cu^{2+} and Ni^{2+} on iron oxide and kaolin and its importance on Ni^{2+} transport in porous media, Colloids Surf., A 211 (2002) 91–102.
[4] D. Mohan, K.P. Singh, Single- and multi-component adsorption of cadmium and zinc using activated carbon derived from bagasse—An agricultural waste, Water Res. 36 (2002) 2304–2318.
[5] K. Huang, Y. Xiu, H. Zhu, Removal of heavy metal ions from aqueous solution by chemically modified mangosteen pericarp, Desalin. Water Treat., doi: 10.1080/19443994.2013.838522.
[6] D. Aderhold, C.J. Williams, R.G.J. Edyvean, The removal of heavy-metal ions by seaweeds and their derivatives, Bioresour. Technol. 58 (1996) 1–6.
[7] N. Balasubramanian, T. Kojima, C.A. Basha, C. Srinivasakannan, Removal of arsenic from aqueous solution using electrocoagulation, J. Hazard. Mater. 167 (2009) 966–969.
[8] M.R. Lasheen, Iman Y. El-Sherif, Y. Dina Sabry, S.T. El-Wakeel, M.F. El-Shahat, Removal of heavy metals from aqueous solution by multiwalled carbon nanotubes: Equilibrium, isotherms, and kinetics, Desalin. Water. Treat., doi: 10.1080/19443994.2013.873880.
[9] N. Mohan, N. Balasubramanian, C.A. Basha, Electrochemical oxidation of textile wastewater and its reuse, J. Hazard. Mater. 147 (2007) 644–651.
[10] H.D. Doan, A. Lohi, V.B.H. Dang, T. Dang-Vu, Removal of Zn^{2+} and Ni^{2+} by adsorption in a fixed bed of wheat straw, Process Saf. Environ. 86 (2008) 259–267.
[11] J.S. Kwon, S.T. Yun, J.H. Lee, S.O. Kim, H.Y. Jo, Removal of divalent heavy metals (Cd, Cu, Pb, and Zn) and arsenic(III) from aqueous solutions using scoria: Kinetics and equilibria of sorption, J. Hazard. Mater. 174 (2010) 307–313.
[12] P.S. Kumar, S. Ramalingam, V. Sathyaselvabala, S.D. Kirupha, S. Sivanesan, Removal of copper (II) ions from aqueous solution by adsorption using cashew nut shell, Desalination 266 (2011) 63–71.
[13] Y. Feng, J. Gong, G. Zeng, Q. Niu, H. Zhang, C. Niu, J. Deng, M. Yan, Adsorption of Cd (II) and Zn (II) from aqueous solutions using magnetic hydroxyapatite nanoparticles as adsorbents, Chem. Eng. J. 162 (2010) 487–494.

[14] F.A. Al-Khaldi, B. Abu-Sharkh, A.M. Abulkibash, M.A. Atieha, Cadmium removal by activated carbon, carbon nanotubes, carbon nanofibers, and carbon fly ash: A comparative study, Desalin. Water Treat., doi: 10.1080/19443994.2013.847805.
[15] A. Murugesan, T. Vidhyadevi, S.S. Kalaivani, M.P. Premkumar, L. Ravikumar, S. Sivanesan, Kinetic and thermodynamic studies on the removal of Zn^{2+} and Ni^{2+} from their aqueous solution using poly(phenylthiourea)imine, Chem. Eng. J. 197 (2012) 368–378.
[16] K. Yogesh Kumar, H.B. Muralidhara, Y. Arthoba Nayaka, J. Balasubramanyam, Low-cost synthesis of mesoporous Zn(II) Sn(II) mixed oxide nanoparticles for the adsorption of dye and heavy metal ion from aqueous solution, Desalin. Water Treat. 52 (2014) 4029–4039.
[17] P.S. Kumar, S. Ramalingam, S.D. Kirupha, A. Murugesan, T. Vidhyadevi, S. Sivanesan, Adsorption behavior of nickel(II) onto cashew nut shell: Equilibrium, thermodynamics, kinetics, mechanism and process design, Chem. Eng. J. 167 (2011) 122–131.
[18] T. Kuila, S. Bose, A.K. Mishra, P. Khanra, N.H. Kim, J.H. Lee, Chemical functionalization of graphene and its applications, Prog. Mater. Sci. 57 (2012) 1061–1105.
[19] C.Y. Su, A.Y. Lu, Y. Xu, F.R. Chen, A.N. Khlobystov, L.J. Li, High-quality thin graphene films from fast electrochemical exfoliation, ACS Nano. 5 (2011) 2332–2339.
[20] L. Fan, C. Luo, M. Sun, H. Qiu, Synthesis of graphene oxide decorated with magnetic cyclodextrin for fast chromium removal, J. Mater. Chem. 22 (2012) 24577–24583.
[21] J. Zhu, R. Sadu, S. Wei, D.H. Chen, N. Haldolaarachchige, Z. Luo, J.A. Gomes, D.P. Young, Z. Guo, Magnetic graphene nanoplatelet composites toward arsenic removal, ECS J. Solid State Sci. Technol. 1 (2012) M1–M5.
[22] F. Liu, S. Chung, G. Oh, T.S. Seo, Three-dimensional graphene oxide nanostructure for fast and efficient water-soluble dye removal, ACS Appl. Mater. Interfaces 4 (2012) 922–927.
[23] J. Zhu, S. Wei, H. Gu, S.B. Rapole, Q. Wang, Z. Luo, N. Haldolaarachchige, D.P. Young, Z. Guo, One-pot synthesis of magnetic graphene nanocomposites decorated with core@double-shell nanoparticles for fast chromium removal, Environ. Sci. Technol. 46 (2012) 977–985.
[24] L. Ai, C. Zhang, Z. Chen, Removal of methylene blue from aqueous solution by a solvothermal-synthesized graphene/magnetite composite, J. Hazard. Mater. 192 (2011) 1515–1524.
[25] J. Guo, R. Wang, W.W. Tjiu, J. Pan, T. Liu, Synthesis of Fe nanoparticles@graphene composites for environmental applications, J. Hazard. Mater. 225–226 (2012) 63–73.
[26] L. Wang, J. Li, Q. Jiang, L. Zhao, Water-soluble Fe_3O_4 nanoparticles with high solubility for removal of heavy-metal ions from waste water, Dalton. Trans. 41 (2012) 4544–4551.
[27] Y.F. Shen, J. Tang, Z.H. Nie, Y.D. Wang, Y. Ren, L. Zuo, Preparation and application of magnetic Fe_3O_4 nanoparticles for wastewater purification, Sep. Purif. Technol. 68 (2009) 312–319.
[28] T. Shahriari, G. Nabi Bidhendi, N. Mehrdadi, A. Torabian, Effective parameters for the adsorption of chromium(III) onto iron oxide magnetic nanoparticle, Int. J. Environ. Sci. Technol. 11 (2014) 349–356.
[29] K.Z. Elwakeel, Removal of arsenate from aqueous media by magnetic chitosan resin immobilized with molybdate oxoanions, Int. J. Environ. Sci. Technol. 11 (4) (2014) 1051–1062.
[30] G. Sheng, J. Li, D. Shao, J. Hu, C. Chen, Y. Chen, X. Wang, Adsorption of copper(II) on multiwalled carbon nanotubes in the absence and presence of humic or fulvic acids, J. Hazard. Mater. 178 (2010) 333–340.
[31] G. Sheng, Y. Li, X. Yang, X. Ren, S. Yang, J. Hu, X. Wang, Efficient removal of arsenate by versatile magnetic graphene oxide composites, RSC Adv. 2 (2012) 12400–12407.
[32] T.N. Narayanan, Z. Liu, P.R. Lakshmy, W. Gao, Y. Nagaoka, D. Sakthi Kumar, J. Lou, R. Vajtai, P.M. Ajayan, Synthesis of reduced graphene oxide–Fe_3O_4 multifunctional freestanding membranes and their temperature dependent electronic transport properties, Carbon 50 (2012) 1338–1345.
[33] K. Zhou, Y. Zhu, X. Yang, C. Li, Preparation and application of mediator-free H_2O_2 biosensors of graphene–Fe_3O_4 composites, Electroanalysis 23 (2011) 862–869.
[34] X. Yang, X. Zhang, Y. Ma, Y. Huang, Y. Wang, Y. Chen, Superparamagnetic graphene oxide–Fe_3O_4 nanoparticles hybrid for controlled targeted drug carriers, J. Mater. Chem. 19 (2009) 2710–2714.
[35] W. Fan, W. Gao, C. Zhang, W.W. Tjiu, J. Pan, T. Liu, Hybridization of graphene sheets and carbon-coated Fe_3O_4 nanoparticles as a synergistic adsorbent of organic dyes, J. Mater. Chem. 22 (2012) 25108–25115.
[36] G. Xie, P. Xi, H. Liu, F. Chen, L. Huang, Y. Shi, F. Hou, Z. Zeng, C. Shao, J. Wang, A facile chemical method to produce superparamagnetic graphene oxide–Fe_3O_4 hybrid composite and its application in the removal of dyes from aqueous solution, J. Mater. Chem. 22 (2012) 1033–1039.
[37] V. Chandra, J. Park, Y. Chun, J.W. Lee, I.C. Hwang, K.S. Kim, Water-dispersible magnetite-reduced graphene oxide composites for arsenic removal, ACS Nano. 4 (2010) 3979–3986.
[38] H.L. Poh, F. Šaněk, A. Ambrosi, G. Zhao, Z.E. Sofer, M. Pumera, Graphenes prepared by Staudenmaier, Hofmann and Hummers methods with consequent thermal exfoliation exhibit very different electrochemical properties, Nanoscale 4 (2012) 3515–3522.
[39] D.C. Marcano, D.V. Kosynkin, J.M. Berlin, A. Sinitskii, Z. Sun, A. Slesarev, L.B. Alemany, W. Lu, J.M. Tour, Improved synthesis of graphene oxide, ACS Nano. 4 (2010) 4806–4814.
[40] K. Zhou, Y. Zhu, X. Yang, C. Li, One-pot preparation of graphene/Fe_3O_4 composites by a solvothermal reaction, New J. Chem. 34 (2010) 2950–2955.
[41] G. Sheng, H. Dong, R. Shen, Y. Li, Microscopic insights into the temperature-dependent adsorption of Eu(III) onto titanate nanotubes studied by FTIR, XPS, XAFS and batch technique, Chem. Eng. J. 217 (2013) 486–494.

[42] G. Sheng, H. Dong, Y. Li, Characterization of diatomite and its application for the retention of radiocobalt: Role of environmental parameters, J. Environ. Radioactiv. 113 (2012) 108–115.
[43] G. Sheng, R. Shen, H. Dong, Y. Li, Colloidal diatomite, radionickel, and humic substance interaction: A combined batch, XPS, and EXAFS investigation, Environ. Sci. Pollut. Res. 20 (2013) 3708–3717.
[44] G. Zolfaghari, A. Esmaili-Sari, M. Anbia, H. Younesi, M.B. Ghasemian, A zinc oxide-coated nanoporous carbon adsorbent for lead removal from water: Optimization, equilibrium modeling, and kinetics studies, Int. J. Environ. Sci. Technol. 10(2) (2013) 325–340.
[45] S. Nethaji, A. Sivasamy, A.B. Mandal, Adsorption isotherms, kinetics and mechanism for the adsorption of cationic and anionic dyes onto carbonaceous particles prepared from *Juglans regia* shell biomass, Int. J. Environ. Sci. Technol. 10(2) (2013) 231–242.
[46] I. Langmuir, The adsorption of gases on plane surfaces of glass, mica and platinum, J. Am. Chem. Soc. 40 (1918) 1361–1403.
[47] H.M.F. Freundlich, Over the adsorption in solution, J. Phys. Chem. 57 (1906) 385–470.
[48] O. Redlich, D.L. Peterson, A useful adsorption isotherm, The J. Phys. Chem. 63 (1959) 1024–1026.
[49] M.J. Temkin, V. Pyzhev, Recent modifications to Langmuir isotherms, Acta. Physicochimica. URSS 12 (1940) 217–225.
[50] S. Lagergren, About the theory of so-called adsorption of soluble substances, Kungliga. Sven. Vetensk. Handl. 24 (1898) 1–39.
[51] Y.S. Ho, G. McKay, Pseudo-second order model for sorption processes, Process. Biochem. 34 (1999) 451–465.
[52] Y.S. Ho, G. McKay, Application of kinetic models to the sorption of copper (II) onto peat, Adsorpt. Sci. Technol. 20 (2002) 797–815.
[53] W.J. Weber, J.C. Morris, Kinetics of adsorption on carbon from solution, J. San. Eng Div. Am. Soc. Civil Eng. 89 (1963) 31–60.
[54] M. Abdel Salam, Removal of heavy metal ions from aqueous solutions with multi-walled carbon nanotubes: Kinetic and thermodynamic studies, Int. J. Environ. Sci. Technol. 10(4) (2013) 677–688.
[55] N. Chubar, J.R. Carvalho, M.J.N. Correia, Cork biomass as biosorbent for Cu(II), Zn(II) and Ni(II), Colloid Surf., A 230 (2003) 57–65.
[56] M.A. Farajzadeh, A.B. Monji, Adsorption characteristics of wheat bran towards heavy metal cations, Sep. Purif. Technol. 38 (2004) 197–207.
[57] E. Malkoc, Ni(II) removal from aqueous solutions using cone biomass of *Thuja orientalis*, J. Hazard. Mater. 137 (2006) 899–908.
[58] S.R. Shukla, R.S. Pai, Adsorption of Cu(II), Ni(II) and Zn(II) on dye loaded groundnut shells and sawdust, Sep. Purif. Technol. 43 (2005) 1–8.
[59] B.S. Gupta, M. Curran, S. Hasan, T.K. Ghosh, Adsorption characteristics of Cu and Ni on Irish peat moss, J. Environ. Manage. 90 (2008) 954–960.
[60] R. Nie, X. Chang, Q. He, Z. Hu, Z. Li, Preparation of p-tert[(dimethylamino)methyl]-calix[4]arene functionalized aminopropylpolysiloxane resin for selective solid-phase extraction and preconcentration of metal ions, J. Hazard. Mater. 169 (2009) 203–209.
[61] S.R. Shukla, R.S. Pai, A.D. Shendarkar, Adsorption of Ni(II), Zn(II) and Fe(II) on modified coir fibres, Sep. Purif. Technol. 47 (2006) 141–147.